




Coexistence of ferromagnetism and antiferromagnetic dimers in topological insulators

Farhan Islam ^{1,2}, Deborah Schlager,¹ Yongbin Lee,¹ Santanu Pakhira ¹, Daniel M. Pajerowski,³
David C. Johnston ^{1,2}, Liqin Ke,¹ David Vaknin,^{1,2} and Robert J. McQueeney^{1,2}

¹*Ames National Laboratory, Ames, Iowa 50011, USA*

²*Department of Physics and Astronomy, Iowa State University, Ames, Iowa 50011, USA*

³*Neutron Scattering Division, Oak Ridge National Laboratory, Oak Ridge, Tennessee 37831, USA*



(Received 2 February 2024; accepted 10 June 2024; published 3 July 2024)

The addition of magnetic impurities in topological insulators (TIs) can drive ferromagnetic order that leads to quantum anomalous Hall transport well below the Curie temperature. The fragility of the quantized regime has been ascribed to the random nature of the magnetic moment distribution. Here, we refine this hypothesis by using inelastic neutron scattering and density-functional theory calculations to show that two antagonistic components define the magnetism in Mn-substituted SnTe, thereby limiting the effectiveness of dilute magnetic TIs. One component is strongly bound antiferromagnetic dimers that compete with ferromagnetic order. The other component consists of undimerized moments where ferromagnetic order develops via long-range interactions.

DOI: [10.1103/PhysRevB.110.014408](https://doi.org/10.1103/PhysRevB.110.014408)

I. INTRODUCTION

The development of ferromagnetic (FM) order in topological insulators (TIs) is key to unlocking the quantum anomalous Hall effect (QAHE) where edge states can carry electrical current without dissipation [1–6]. The first successful approach to demonstrate the QAHE introduced ferromagnetism into nonmagnetic and nontrivial topological insulators such as Bi₂Te₃ and Sb₂Te₃ through the substitution of low concentrations of magnetic ions [4,7–11]. Similar to dilute magnetic semiconductors, small concentrations of ions ($\leq 5\%$) are capable of introducing FM order, which presumably occurs through long-range interactions [9,12–22]. The random nature of magnetic substitution is hypothesized to introduce fundamental limitations to the temperature onset of the QAHE, which motivated the search for intrinsic magnetic topological insulators, leading to the discovery of MnBi₂Te₄ [23–34]. However, a detailed understanding of the magnetic interactions in the dilute case and why QAHE is suppressed remains elusive [35,36]. One may even question how long-range magnetic interactions, necessary for FM order in dilute systems, can be mediated without a high density of conduction electrons.

Recent inelastic-neutron-scattering (INS) measurements raise additional questions by finding strong antiferromagnetic (AF) interactions in paramagnetic (PM) Sb₂Te₃ [37] and SnTe [38] topological insulators with low concentrations of Mn substitution. AF spin dimers form between next-nearest-neighbor (NNN) Mn atoms possessing Mn-Te-Mn linear bonds, following the well-known Goodenough-Kanamori rules [39]. The AF interactions are found to be many times stronger than any FM couplings and form tightly bound dimer-singlet states. This suggests the existence of a two-component magnetic system where AF dimer singlets coexist with weakly coupled and undimerized Mn ions. It is an interesting and fundamental problem to understand how FM order develops when the Mn concentration is increased beyond the threshold for FM order.

SnTe is one of the first known examples of a topological crystalline insulator [40–45]. In this system, surface electronic states are protected by time-reversal and crystalline symmetries. SnTe adopts a cubic rock-salt structure [46] and FM order with the substitution of Mn for Sn [47–49]. FM order develops above a critical composition of about 5%, where the exact compositional crossover depends on thermal treatment [38]. The underlying mechanism responsible for the development of FM order is still debated.

Here, we extend previous studies of 5% Mn-doped SnTe [38] to 10% Mn-doped SnTe, and for completeness, we extensively compare the two systems. Our study aims to unravel the characteristics of the magnetic interactions that drive the development of ferromagnetism in this 10% Mn-doped SnTe. AF dimer excitations persist at these compositions and are found to be split by the average molecular-field of FM-ordered Mn ions. We also observe a FM resonance which provides a direct measure of the molecular field strength and tracks the FM order parameter. These studies enforce the two-component hypothesis in the PM and FM regimes for both SnTe and (Bi,Sb)₂Te₃ dilute magnetic TI families. In the two-component model, undimerized Mn ions are coupled by weak, but long-ranged, magnetic interactions that form a backbone of the FM order. The strong AF dimers are weakly polarized through interaction with the molecular field of the undimerized spins, which limits the global magnetization and introduces spatial inhomogeneities.

The formation of Mn-Mn AF dimers may explain why the QAHE has only been observed for Cr- and V-substituted TIs [50], but never with Mn substitutions. To investigate this point, we conducted density-functional-theory (DFT) calculations of the pairwise magnetic interactions between two M ions in SnTe where $M = \text{V, Cr, Mn}$. In the case of Mn, DFT finds that the NNN dimer is strongly AF, in agreement with experiment, but fails to reproduce the additional FM interactions between other pairs that are needed for the development of long-range FM order. Similar to Mn, the NNN V-V dimer also

exhibits a weaker AF dimer coupling, but nearest-neighbor (NN) and other couplings favor ferromagnetism. Surprisingly, all couplings with Cr doping are FM with NNN Cr-Cr dimer exhibiting very strong FM coupling, consistent with experimental reports of high-temperature FM order in Cr-substituted SnTe [51–53]. These results suggest that Cr and V substitutions are more favorable than Mn to host robust topological states with broken time-reversal symmetry.

II. METHODS

A. Sample synthesis and characterization

Polycrystalline samples of $\text{Sn}_{1-x}\text{Mn}_x\text{Te}$ (where $x = 0, 0.05$, and 0.1) were synthesized using solid-state reaction from stoichiometric quantities of Sn, Mn, and Te. Analysis of scanning electron microscopy and energy-dispersive spectroscopy show the $x = 0.1$ sample to be single phase with a composition of $x = 0.10(1)$ and x-ray powder diffraction measurements confirm the SnTe structure. Magnetization measurements were carried out using a Quantum Design MPMS magnetometer. For more details, see the Supplemental Material (SM) [54].

B. Inelastic neutron scattering

Inelastic neutron scattering measurements were performed on all three samples of $\text{Sn}_{1-x}\text{Mn}_x\text{Te}$ with $x = 0, 0.05$, and 0.1 using the Cold Neutron Chopper Spectrometer (CNCS) spectrometer at the Spallation Neutron Source at Oak Ridge National Laboratory. Incident neutron energies of $E_i = 1.55$ and 3.32 meV were chosen and the samples were measured at several temperatures from 2 K to 20 K. The INS intensity is reported as $I(Q, E)$, which is proportional to the spin-spin correlation function between Mn ions.

III. EXPERIMENTAL DATA

The $\text{Sn}_{1-x}\text{Mn}_x\text{Te}$ sample remains paramagnetic for $x = 0.05$ and displays no long-range FM order, as reported previously [38]. Conversely, the $x = 0.1$ sample does display FM order with a Curie temperature $T_C \approx 12$ K, as observed from magnetic susceptibility and magnetization measurements shown in Fig. 1(a). Other details of sample synthesis and characterization are given in the SM [54].

We performed inelastic neutron scattering experiments on powders of $\text{Sn}_{1-x}\text{Mn}_x\text{Te}$ with $x = 0, 0.05$, and 0.1 using the CNCS at the Spallation Neutron Source. Measurements were performed at several temperatures with incident neutron energies of $E_i = 1.55$ and 3.32 meV. Figure 1(b) shows elastic-neutron-scattering data from the $x = 0.1$ sample at several temperatures after subtraction of the $T = 20$ K data. There is clear evidence for long-range FM ordering that contributes to the (111) reflection where the nuclear contribution is very weak (see SM [54] and Refs. [55,56] therein). The integrated intensity of the FM (111) peak is shown in Fig. 1(c) and displays mean-field-like evolution with an estimated $T_C = 12.7(7)$ K.

As reported previously, INS data from the paramagnetic $x = 0.05$ composition contain strongly coupled AF dimers with exchange coupling of $\mathcal{J}_2 \approx -0.58$ meV [38]. Figures 2(a) and 2(c) display INS data for $x = 0.05$ where the

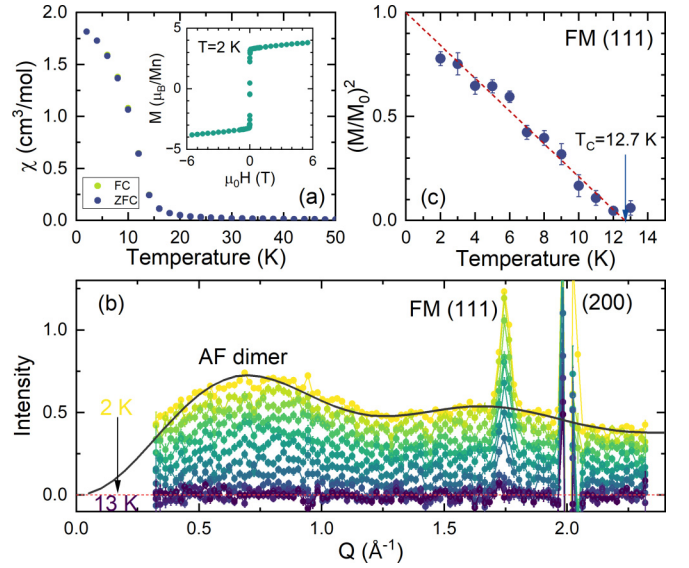


FIG. 1. Long-range ferromagnetic order in $\text{Sn}_{0.9}\text{Mn}_{0.1}\text{Te}$. (a) Field-cooled (FC) and zero-field-cooled (ZFC) magnetic susceptibility measured in a magnetic field $H = 0.1$ T showing a smeared onset of ferromagnetic order near 15 K. The inset shows the low-temperature magnetization vs field that is characteristic of a soft ferromagnet. (b) Elastic neutron-scattering intensity (integrated from $E = -0.05$ to 0.05 meV) at $E_i = 3.32$ meV as a function of momentum transfer plotted for several temperatures after subtracting 20 K data. The magnetic component of the (111) reflection is indicated, as well as broad diffuse scattering consistent with NNN antiferromagnetic dimers. The data are not offset. The solid black line is the calculated average structure factor for an NNN AF dimer. (c) Ferromagnetic order parameter obtained from the integrated intensity of the magnetic (111) reflection. M_0 is obtained from the linear fit (red dashed line) at $T = 0$ K with arbitrary units.

principal feature is a dimer spin-state transition from the $S = 0$ singlet ground state to the $S = 1$ triplet excited state with energy $E = |\mathcal{J}_2|$. The excitation has a characteristic Q -dependent dimer structure factor, as shown in Fig. 2(d). The dimers consist of NNN Mn ions where linear Mn-Te-Mn bonds mediate strong AF superexchange coupling. At energies below 0.2 meV, Figs. 2(a) and 2(c) indicate that strong quasielastic magnetic fluctuations are present, as expected for a paramagnet that is close to FM order. Figure 2(e) shows that the quasielastic magnetic fluctuations are strongly enhanced at small Q for $x = 0.05$, which is a signature of FM character.

The spectrum of the FM-ordered $x = 0.1$ sample is shown in Figs. 2(b) and 2(c). The quasielastic fluctuations are absent and the inelastic spectrum now consists of contributions from both AF dimers and FM excitations. AF dimers survive in the FM-ordered state, but their spectral weight is smeared out and a strong component shifts to low energies (<0.25 meV). Analysis of the structure factor below 0.25 meV in Fig. 2(e) shows a dominant dimer contribution. Dimer scattering also appears in the elastic scans shown in Fig. 1(b), which could indicate that static AF (spin-glass) correlations are present [48]. Broad spectral features between 0.5 and 1.0 meV in Figs. 2(b) and 2(d) consist of overlapping contributions from dimers and FM-ordered Mn ions. The FM correlations in

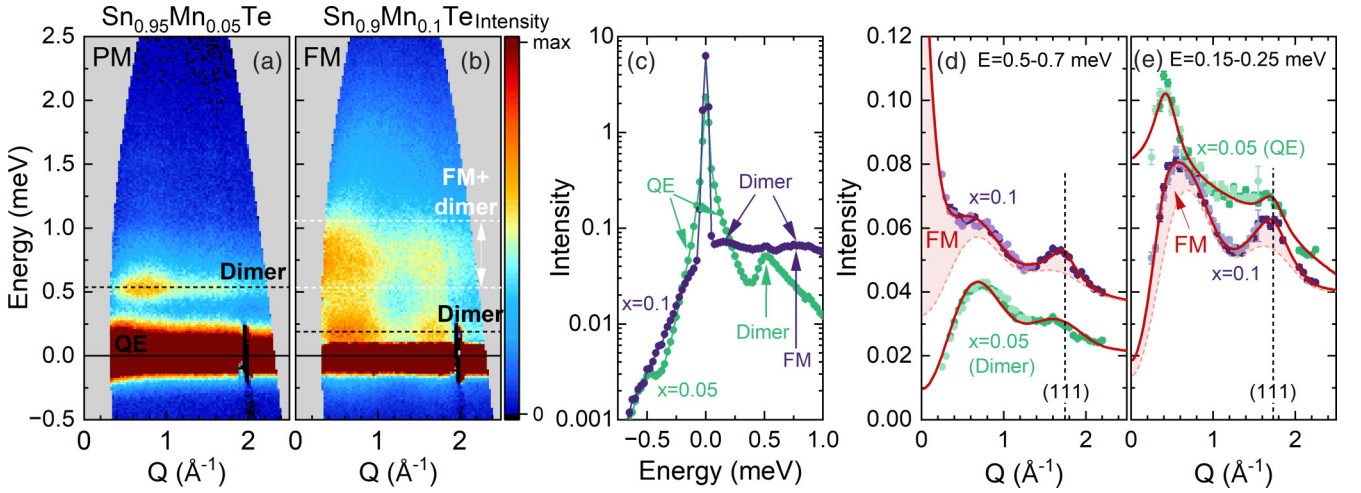


FIG. 2. Low-temperature magnetic excitations in $\text{Sn}_{1-x}\text{Mn}_x\text{Te}$. Powder inelastic-neutron-scattering spectra measured at $T = 2\text{ K}$ and $E_i = 3.32\text{ meV}$ for (a) the paramagnetic $x = 0.05$ sample and (b) the ordered ferromagnetic $x = 0.1$ sample. Horizontal lines or regions highlight quasielastic (QE), dimer, and FM resonance excitations. (c) Energy spectra of $x = 0.05$ (green) and $x = 0.1$ (blue) samples measured with $E_i = 1.55\text{ meV}$ and averaged over the full Q range. Arrows highlight spectral features seen in (a) and (b). Q dependence of magnetic spectra of the $x = 0.05$ (green) and $x = 0.1$ (purple) samples at (d) $E = 0.5\text{--}0.7\text{ meV}$ and (e) $E = 0.15\text{--}0.25\text{ meV}$. In (d) and (e) light (dark) symbols are measured with $E_i = 1.55$ (3.32) meV, respectively. Solid red lines are fits to dimer plus ferromagnetic line shapes, as described in the Supplemental Material. The dashed pink line shows the dimer contribution to the $x = 0.1$ sample data and the shaded region is the ferromagnetic contribution.

this energy range increase sharply as $Q \rightarrow 0$ and also form a weaker peak at the (111) Brillouin zone center.

Next, we describe a characteristic excitation of the long-range-ordered dilute magnet, identified as a FM resonance. Deep within the ordered state, the FM resonance contributes to a broad, low-temperature peak at 0.8 meV as described above and shown in Fig. 3(a). As the temperature is increased, Figs. 3(a) and 3(c) show that the FM resonance shifts to lower energies and forms a quasielastic feature above T_C . The fitted values of the FM resonance energy (Δ) evolve

according to a mean-field-like magnetic order parameter ($\Delta = \Delta_0 \sqrt{1 - T/T_C}$) shown in Fig. 3(c). As described below, the resonance energy is associated with the Zeeman splitting of the Mn spin states in the self-consistent molecular field of surrounding Mn ions.

IV. TWO-COMPONENT MAGNETISM MODEL

Mn-doped SnTe and other dilute magnetic topological insulators are unusual ferromagnets because the strongest

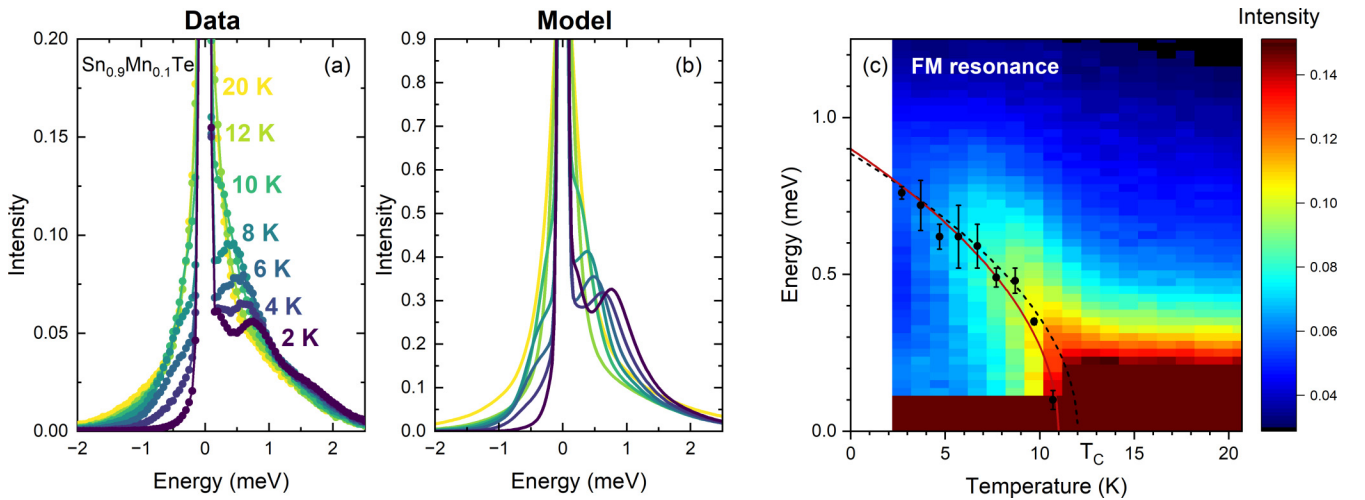


FIG. 3. Ferromagnetic resonance excitation. (a) The magnetic energy spectrum averaged over $Q = 0.7\text{--}1.5\text{ \AA}$ for several temperatures showing the evolution of the FM resonance peak. (b) Calculations of the magnetic spectrum using the two-component magnetism model. (c) Image plot of the magnetic spectrum data from (a) for all temperatures. A fit (dashed line) to the resonance peak (circles) is shown together with a fit (red line) to a mean-field-like order parameter with $T_C = 11\text{ K}$ and $\Delta_0 = 0.9\text{ meV}$ as described in the text. The dashed line is the mean-field order parameter with $T_C = 12\text{ K}$ and $\Delta_0 = 3k_B T_C / (s + 1)$.

TABLE I. Parameters of the two-component model. x is the concentration of Mn, f_u (f_d) is the undimerized (dimerized) fraction of Mn, \mathcal{J}_2 is the AF dimer exchange, T_C is the Curie temperature, and γ (Γ) is the inelastic (quasielastic) width.

x	f_u	f_d	\mathcal{J}_2 (meV)	T_C (K)	γ (meV)	Γ (meV)
0.05	0.735	0.180	-0.58	0	0.28	0.07
0.10	0.531	0.209	-0.58	12.7	0.85	0.28

interaction is AF. Here, we describe a simple two-component magnetic model that differentiates between undimerized Mn ions (spins with no NNN neighbors), those with one NNN neighbor (a dimer), and those with more than one NNN neighbor (trimers and larger AF clusters).

A. Random magnetic alloy

For the random substitution of xN Mn ions onto N Sn sites, the fraction of undimerized Mn ions is $f_u = (1-x)^6 \approx 53\%$ (the total number of undimerized Mn ions $N_u = Nx f_u$). The fraction of Mn ions that participate in a NNN dimer is $f_d = 6x(1-x)^{10} \approx 21\%$, forming $N_d = Nx f_d/2$ total dimers (ignoring NN occupations) for $x = 0.1$. All other Mn ions ($N_c = Nx - N_u - 2N_d$) are part of larger NNN clusters which have a more complicated spectrum that is assumed to form a background scattering. See Table I for more details.

FM order can only develop in dilute systems when the concentration of magnetic ions exceeds the percolation threshold. For an fcc sublattice with NN FM interactions, the site percolation threshold of $x_p = 0.198$ is insufficient to establish order. Longer-range interactions are needed. For example, $x_p \approx 0.056$ for interactions up to four nearest neighbors (excluding the NNN shell) [57], which is easily exceeded in the $x = 0.1$ sample.

B. Two-component Hamiltonian

We hypothesize that the undimerized spins are coupled by long-range interactions that form a FM-ordered backbone when the Mn concentration exceeds the percolation threshold. AF NNN dimers are only weakly polarized by coupling to the FM-ordered spins.

Within a mean-field approximation, the undimerized and dimerized Hamiltonians become decoupled (see the Appendix for a derivation) and are given by

$$\mathcal{H}_u = -g\mu_B B_{\text{MF}} s^z \quad (1)$$

$$\mathcal{H}_d = -\mathcal{J}_2 \mathbf{s}_1 \cdot \mathbf{s}_2 + \mathcal{H}_{u,1} + \mathcal{H}_{u,2}, \quad (2)$$

where B_{MF} is the molecular field generated by the undimerized spins and $\mathcal{J}_2 = -0.58$ meV [38] is the AF coupling between NNN dimers. In Eq. (2), $\mathcal{H}_{u,i}$ is the interaction of the molecular field with spin i in the NNN dimer [Eq. (1)]. The molecular field is a sum over coordination shells (k) with fcc coordination number z_k which excludes the NNN ($k = 2$) shell, given by

$$g\mu_B B_{\text{MF}} = xs \sum_{k \neq 2} z_k \mathcal{J}_k. \quad (3)$$

The average molecular field in the ground state can be estimated from the Curie temperature $T_C = s(s+1)(x \sum_{k \neq 2} z_k \mathcal{J}_k)/3k_B \approx 12.7$ K, resulting in a value of $g\mu_B B_{\text{MF}}(0) = 3k_B T_C/(s+1) \approx 0.95$ meV. Within mean-field approximation, the molecular field is $B_{\text{MF}} = 0$ above T_C and

$$g\mu_B B_{\text{MF}}(T) = g\mu_B B_{\text{MF}}(0) \sqrt{1 - \frac{T}{T_C}} \quad (4)$$

below T_C . Figures 1(b) and 3(c) show that both the order parameter and FM resonance follow a mean-field form and we can associate $\Delta_0 = g\mu_B B_{\text{MF}}(0)$ and $\Delta = g\mu_B B_{\text{MF}}(T)$.

For the undimerized spin s , the eigenstates of \mathcal{H}_u are the conventional $|s, m\rangle$ spin states projected along the molecular field direction (chosen to be the z axis) and with Zeeman energy $E_m = -g\mu_B B_{\text{MF}} m$. The level spectrum for $s = 5/2$ is shown in Fig. 4(b).

For the AF dimer with $B_{\text{MF}} = 0$, the energy levels depend only on the total spin $S = 0, \dots, 2s$ of the dimer $E_S = -\frac{\mathcal{J}_2}{2}[S(S+1) - 2s(s+1)]$ and each level has a degeneracy of $2S+1$. The dimer spin states can be written in the m_1, m_2 basis as $|\mathcal{S}, \mathcal{M}\rangle = \sum_{m_1, m_2} c_{m_1, m_2}^{\mathcal{S}, \mathcal{M}} |s, m_1\rangle |s, m_2\rangle$, where $c_{m_1, m_2}^{\mathcal{S}, \mathcal{M}}$ is a Clebsch-Gordan coefficient. The molecular field acting on the dimer will result in a Zeeman splitting of the dimer energy levels, but \mathcal{M} remains a good quantum number, as shown in Fig. 4(b).

V. DATA ANALYSIS

Using the Hamiltonians (1) and (2), the INS intensity of the two-component model is given by

$$I(Q, E) = N_u I_u(Q, E) + N_d I_d(Q, E) + N_c I_c, \quad (5)$$

where the intensity from larger AF clusters (I_c) is assumed to form a featureless background and is not considered further. The explicit forms for I_u and I_d are given in the Appendix.

Figures 4(d) and 4(e) show calculations of the low-temperature spectra for $x = 0.05$ and $x = 0.1$ samples with the parameters given in Table I. This simple approximation does not include spatial correlations of the FM-ordered ions, and is of limited value in analyzing the Q dependence of the excitations. However, Figs. 3 and 4 show that the model reproduces the spectral features of both samples with only three parameters: the Mn concentration (x), the AF dimer exchange (\mathcal{J}_2), and the Curie temperature (T_C), where the latter parameter determines the strength and temperature dependence of the molecular field. We also include parameters, i.e., γ and Γ in Table I, that represent spectral broadening (see SM [54]).

The two-component model associates the FM resonance energy with the Zeeman splitting of the undimerized Mn ions in the molecular field. As neutron scattering observes transitions with $\Delta m = \pm 1$, the resonance measures directly the average molecular field at $T < T_C$ ($\Delta = g\mu_B B_{\text{MF}}(T)$), as shown in Fig. 4(b). Figure 3 confirms the resonance energy $g\mu_B B_{\text{MF}}(0) \approx 0.95$ meV and the temperature dependence of the FM resonance follows the two-component mean-field model.

Dimer excited states are also split by the molecular field and can contribute to the FM resonance intensity [red arrow

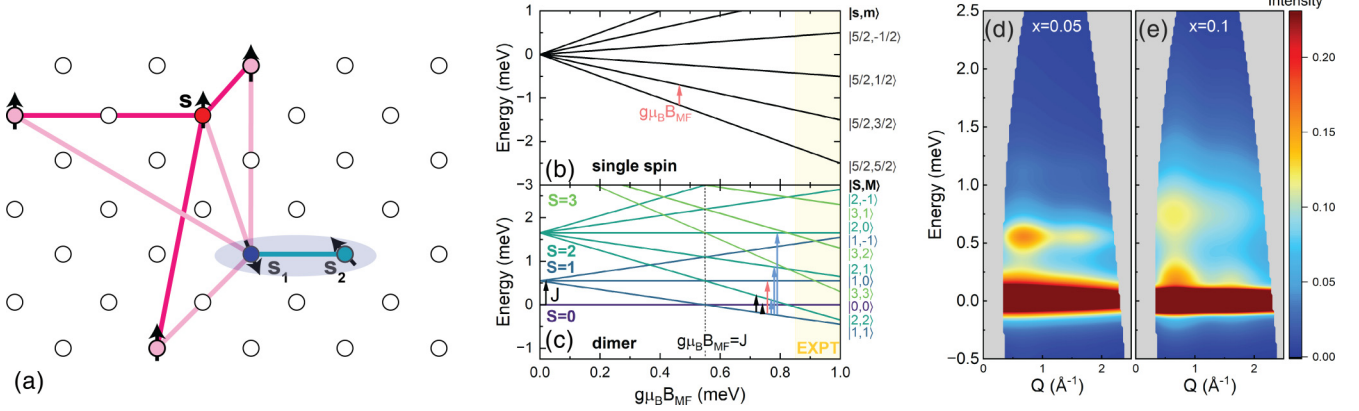


FIG. 4. Two-component magnetic model. (a) Depiction of the interactions of an undimerized Mn spin (red circle) with other undimerized spins (pink circles) and interactions of a dimerized spin (blue circle) with other dimerized (cyan) and undimerized spins. (b) Level diagram for a single $s = 5/2$ spin in the molecular field (B_{MF}) of other undimerized spins. (c) The level diagram of an antiferromagnetic dimer with exchange coupling \mathcal{J}_2 in a molecular field. Vertical arrows show dipole-allowed $S = 0$ to 1 (black) and $S = 1$ to 2 (blue) dimer spin state transitions and $\Delta S = 0$ or $\Delta s = 0$ Zeeman transitions (red) out of the ground state. The vertical dashed line in (c) marks level crossing into the $S = 1$ dimer ground state and the yellow area highlights the approximate experimental value of the ground-state molecular field strength. Two-component model calculations of the inelastic neutron scattering spectrum at $T = 2.2$ K for (d) $x = 0.05$ and (e) $x = 0.1$ using the parameters in Table I.

in Fig. 4(c)]. The dimer level diagram also indicates that the molecular field is sufficiently strong at low temperatures to induce a level crossing to $|\mathcal{S}, \mathcal{M}\rangle = |1, 1\rangle$ ground state. This level crossing creates intense dimer excitations at low energies, corresponding to $|1, 1\rangle \rightarrow |0, 0\rangle$ and $|1, 1\rangle \rightarrow |2, 2\rangle$ spin-state transitions [black arrows in Fig. 4(c)]. Higher-energy dimer excitations [blue arrows in Fig. 4(c), such as $|1, 1\rangle \rightarrow |2, 0\rangle$] create a broad spectrum of dimer excitations up to 1 meV or more.

VI. FIRST-PRINCIPLES CALCULATIONS

Dimer singlet formation is surprisingly ubiquitous in all Mn- and Te-based topological insulators. Strongly coupled AF Mn-Te-Mn dimers form in Mn-substituted Sb_2Te_3 [37] and are known to form in MnBi_2Te_4 and MnSb_2Te_4 intrinsic AF-TI when antisite mixing defects are present [58]. In each case, singlet formation is tied to the presence of linear Mn-Te-Mn bonds that foster strong AF superexchange. However, one caveat is that there are no known observations of the QAHE in Mn-substituted dilute magnetic TIs, suggesting that AF dimer formation is deleterious. On the other hand, Cr- and V-substituted TIs have demonstrated QAHE [50], so it is reasonable to ask whether AF dimer formation can also be found in these compounds. Although our experimental and theoretical work focuses on Mn, we conduct DFT calculations to also evaluate the pairwise exchange couplings between two M ions in SnTe where $M = \text{Mn}, \text{V},$ or Cr.

Our calculations are based on constructing a $3 \times 3 \times 3$ SnTe supercell composed of 216 atoms, with a pair of Sn sites substituted by two $3d$ transition-metal (M) ions to form a dimer. Nine configurations of M - M dimers with different bond lengths are considered by substituting on different Sn sites. The resulting M concentration of our model $< 1\%$ is much lower than in experimental samples, and we disregard the possible influence of nearby impurities on the magnetic interaction within one dimer, which may be present in real

samples. For each dimer, the energies of FM (E_{FM}) and AFM (E_{AFM}) configurations were calculated to estimate the dimer exchange coupling. Further details of the DFT calculations can be found in the SM [54] (see also Refs. [59–62] therein).

Figures 5(a) and 5(b) show the magnetic energy of the dimers, calculated using nonrelaxed and relaxed crystal structures, respectively. Both show a prominent minimum at the NNN position for Mn, confirming the strong AF NNN coupling observed experimentally. Notably, without relaxation, V and Mn dimers exhibit nearly identical behavior, demonstrating a significant AF coupling for the NNN dimer, while all

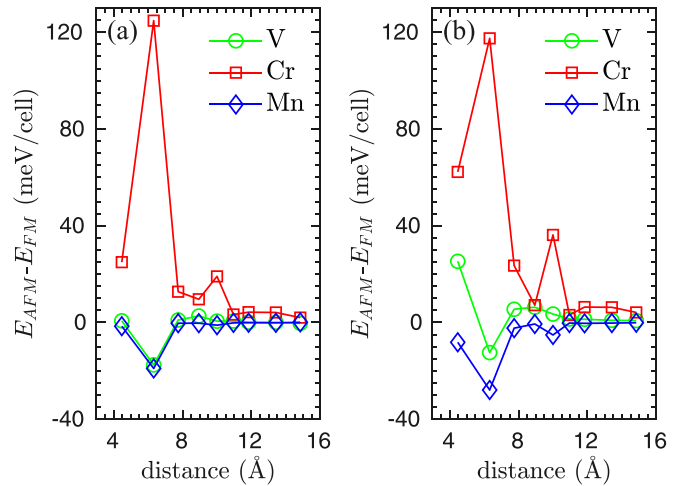


FIG. 5. Dimer magnetic energy as a function of dimer length calculated using the (a) nonrelaxed and (b) relaxed crystal structures. The magnetic energy is defined as the difference between the AFM and FM configurations, $E_{AFM} - E_{FM}$. For Mn dimers and V dimers without structural relaxation, only the NNN dimer shows a similarly large AFM coupling, while all other dimer configurations show negligible magnetic coupling. In contrast, Cr dimers exhibit an overall large FM coupling, especially for the NNN dimer.

other dimer configurations show negligible coupling. In contrast, the interaction between NNN Cr differs markedly from that of V and Mn counterparts, displaying a strong overall FM coupling. This remarkable difference can be traced back to the e_g -orbital filling and degeneracies, as explained in the SM [54] (see also Refs. [63–67] therein). Relaxation of the structure affects the magnetic coupling between two M atoms for the shorter-distance dimer configurations, as shown in Figs. 5(a) and 5(b). The AFM coupling for the NNN V-V dimer becomes weaker than that of the Mn-Mn dimer. Overall, the dominant AFM interaction for the NNN Mn-Mn dimer aligns with experiments and previous observations [37,38]. The FM coupling of Cr is also consistent with previous experiments for both bulk [51,53] and film [52] samples, where Cr-doped SnTe is found to be FM with a high Curie temperature. Further evaluation of the evolution of magnetic interactions using the band-filling model [63] is provided in the SM [54] (see also Refs. [63–67] therein).

VII. CONCLUSION

Mn-doped SnTe develops long-range FM order despite the fact that the largest pairwise magnetic interactions are AF. The maximum magnetic interaction energy of the NNN coordination shell is $6\mathcal{J}_2 = -3.5$ meV, whereas all other shells have $\sum_{k \neq 2} z_k \mathcal{J}_k = 3.8$ meV. Therefore, the overall interaction slightly favors ferromagnetism within a mean-field treatment. However, T_C is determined only by the FM exchange couplings, not the total (which would result in $T_C \approx 1$ K). This justifies the essential premise of the two-component model where the formation of NNN AF dimer singlets only weakly perturbs the development of FM order.

In the two-component model, although T_C is weakly affected by dimer formation, the overall magnetization is suppressed as a result of dimer formation. The level crossing of the dimer in the molecular field of the undimerized spins (into the $|1, 1\rangle$ state) results in a weak magnetization of $g\mu_B \langle \mathcal{M} \rangle = 2\mu_B$ per Mn-Mn dimer. The magnetization per Mn expected from the two-component model at $T = 0$ is $M \approx (5\mu_B)f_u + (2\mu_B)f_d/2 = 2.8\mu_B$, which is close to the measured value of $3.2\mu_B$ in Fig. 1(a).

Despite the success of the two-component model, it is clear that it does not include spatial correlations which are complicated by the presence of both competing magnetic interactions and chemical disorder. Thus, the model is incapable of describing any short-range order, such as spin-glass or cluster formation. Such disorder has been reported previously [48] and is hinted upon in the large quasi-static diffuse scattering observed in the elastic channel [Fig. 1(b)]. The two-component model also ignores the collective character of FM excitations which are expected to form damped magnons as observed in Mn-substituted Bi_2Te_3 [20]. Future measurements on single-crystal samples should be able to address these key details.

DFT calculations confirm NNN AFM Mn-Mn coupling, consistent with our experimental results. While strong AF interactions may prevent the development of the QAHE in Mn-substituted samples, the results from DFT calculations suggest that AF dimer singlets form in V-substituted topological insulators, where the QAHE has been observed. However,

DFT calculations also suggest that V-substituted samples have larger overall FM interactions that support a robust FM order. The DFT results imply that Cr substitution results in strong and long-range FM pairwise interactions, making it an optimal candidate for the development of topological surface states. Overall, these results point to the fundamental chemical barriers that may prevent the development of robust ferromagnetism in Te-based topological insulators. New routes that employ magnetic substitutions to discover Chern and axion insulating topological states are needed to carefully explore crystal structures that avoid these deleterious configurations.

The supporting data for this article are openly available from the Harvard Dataverse [68].

ACKNOWLEDGMENTS

The work at the Ames National Laboratory was supported by the U.S. Department of Energy (USDOE), Office of Basic Energy Sciences, Division of Materials Sciences and Engineering. Ames National Laboratory is operated for the USDOE by Iowa State University under Contract No. DE-AC02-07CH11358. A portion of this research used resources at the Spallation Neutron Source, which is a USDOE Office of Science User Facility operated by the Oak Ridge National Laboratory.

APPENDIX: DERIVATION OF THE TWO-COMPONENT MEAN-FIELD HAMILTONIAN

The magnetic Hamiltonian for dilute and randomly disordered Mn is

$$\mathcal{H} = - \sum_{i,j} \rho_i \rho_j \mathcal{J}_{ij} \mathbf{s}_i \cdot \mathbf{s}_j, \quad (\text{A1})$$

where the sum is over all Sn lattice sites (i) and $\rho_i = 0$ or 1 represents the random Mn occupancy of site i ($\sum_i \rho_i = Nx$). A full quantum treatment of the random magnetic lattice is challenging, so we break this sum up into coordination shells (k), each consisting of z_k unique bond vectors (\mathbf{R}). We explicitly separate out the NNN ($k = 2$) shell with strong AF exchange coupling $\mathcal{J}_2 < 0$. The configurationally averaged Hamiltonian (without double-counting of exchange bonds) becomes

$$\begin{aligned} \mathcal{H} = & -Nx f_u \mathbf{s} \cdot \left(x \sum_{k \neq 2} \sum_{\mathbf{R}=1}^{z_k} \mathcal{J}_k \mathbf{s}_{\mathbf{R}} \right) \\ & - Nx f_d \left[\mathcal{J}_2 \mathbf{s}_1 \cdot \mathbf{s}_2 + (\mathbf{s}_1 + \mathbf{s}_2) \cdot \left(x \sum_{k \neq 2} \sum_{\mathbf{R}=1}^{z_k} \mathcal{J}_k \mathbf{s}_{\mathbf{R}} \right) \right] \\ & + \mathcal{O}(f_c), \end{aligned} \quad (\text{A2})$$

where \mathbf{s} are undimerized spins and $\mathbf{s}_{1,2}$ are dimerized spins, and f_u and f_d are the probability that a Mn ion does not participate or participates in the NNN dimer, respectively. Larger NNN spin clusters [of order $\mathcal{O}(f_c)$] are not enumerated.

Within a mean-field approximation, the remaining sum is the molecular field generated by the undimerized spins. Assuming the saturated magnetization lies along the z axis,

$\mathbf{B}_{\text{MF}} = B_{\text{MF}}\hat{z}$ with average magnitude

$$g\mu_{\text{B}}B_{\text{MF}} = xs \sum_{k \neq 2} z_k \mathcal{J}_k. \quad (\text{A3})$$

The first eight fcc coordination shells have coordination numbers of $z_k = [12, 6, 24, 12, 24, 8, 48, 6]$.

The decoupled Hamiltonians for the single spin and dimer are

$$\mathcal{H}_{\text{u}} = -g\mu_{\text{B}}B_{\text{MF}}s^z \quad (\text{A4})$$

$$\mathcal{H}_{\text{d}} = -\mathcal{J}_2 \mathbf{s}_1 \cdot \mathbf{s}_2 + \mathcal{H}_{\text{u},1} + \mathcal{H}_{\text{u},2}. \quad (\text{A5})$$

In the mean-field approximation, the magnetization of undimerized ions is given by

$$M(T) = g\mu_{\text{B}}\langle s \rangle = g\mu_{\text{B}}s \sqrt{1 - \frac{T}{T_{\text{C}}}}. \quad (\text{A6})$$

This can be used to obtain the temperature dependence of the molecular field

$$g\mu_{\text{B}}B_{\text{MF}}(T) = \langle s \rangle x \sum_{k \neq 2} z_k \mathcal{J}_k = g\mu_{\text{B}}B_{\text{MF}}(0) \sqrt{1 - \frac{T}{T_{\text{C}}}}. \quad (\text{A7})$$

-
- [1] X.-L. Qi, Y.-S. Wu, and S.-C. Zhang, Topological quantization of the spin Hall effect in two-dimensional paramagnetic semiconductors, *Phys. Rev. B* **74**, 085308 (2006).
- [2] X.-L. Qi, T. L. Hughes, and S.-C. Zhang, Topological field theory of time-reversal invariant insulators, *Phys. Rev. B* **78**, 195424 (2008).
- [3] C. Liu, T. L. Hughes, X.-L. Qi, K. Wang, and S.-C. Zhang, Quantum spin Hall effect in inverted type-II semiconductors, *Phys. Rev. Lett.* **100**, 236601 (2008).
- [4] R. Yu, W. Zhang, H.-J. Zhang, S.-C. Zhang, X. Dai, and Z. Fang, Quantized anomalous Hall effect in magnetic topological insulators, *Science* **329**, 61 (2010).
- [5] K. Nomura and N. Nagaosa, Surface-quantized anomalous hall current and the magnetoelectric effect in magnetically disordered topological insulators, *Phys. Rev. Lett.* **106**, 166802 (2011).
- [6] J. G. Checkelsky, R. Yoshimi, A. Tsukazaki, K. S. Takahashi, Y. Kozuka, J. Falson, M. Kawasaki, and Y. Tokura, Trajectory of the anomalous Hall effect towards the quantized state in a ferromagnetic topological insulator, *Nat. Phys.* **10**, 731 (2014).
- [7] H. Zhang, C.-X. Liu, X.-L. Qi, X. Dai, Z. Fang, and S.-C. Zhang, Topological insulators in Bi_2Se_3 , Bi_2Te_3 and Sb_2Te_3 with a single Dirac cone on the surface, *Nat. Phys.* **5**, 438 (2009).
- [8] C.-Z. Chang *et al.*, Experimental observation of the quantum anomalous Hall effect in a magnetic topological insulator, *Science* **340**, 167 (2013).
- [9] J. Zhang, C.-Z. Chang, P. Tang, Z. Zhang, X. Feng, K. Li, L.-l. Wang, X. Chen, C. Liu, W. Duan, K. He, Q.-K. Xue, X. Ma, and Y. Wang, Topology-driven magnetic quantum phase transition in topological insulators, *Science* **339**, 1582 (2013).
- [10] J.-M. Zhang, W. Ming, Z. Huang, G.-B. Liu, X. Kou, Y. Fan, K. L. Wang, and Y. Yao, Stability, electronic, and magnetic properties of the magnetically doped topological insulators Bi_2Se_3 , Bi_2Te_3 and Sb_2Te_3 , *Phys. Rev. B* **88**, 235131 (2013).
- [11] C.-Z. Chang, W. Zhao, D. Y. Kim, H. Zhang, B. A. Assaf, D. Heiman, S.-C. Zhang, C. Liu, M. H. W. Chan, and J. S. Moodera, High-precision realization of robust quantum anomalous Hall state in a hard ferromagnetic topological insulator, *Nat. Mater.* **14**, 473 (2015).
- [12] T. Dietl and H. Ohno, Dilute ferromagnetic semiconductors: Physics and spintronic structures, *Rev. Mod. Phys.* **86**, 187 (2014).
- [13] J. S. Dyck, P. Hájek, P. Lošťák, and C. Uher, Diluted magnetic semiconductors based on $\text{Sb}_{2-x}\text{V}_x\text{Te}_3$ ($0.01 < x < 0.03$), *Phys. Rev. B* **65**, 115212 (2002).
- [14] J. Choi, S. Choi, J. Choi, Y. Park, H.-M. Park, H.-W. Lee, B.-C. Woo, and S. Cho, Magnetic properties of Mn-doped Bi_2Te_3 and Sb_2Te_3 , *Physica Status Solidi B* **241**, 1541 (2004).
- [15] J. S. Dyck, Č. Drašar, P. Lošťák, and C. Uher, Low-temperature ferromagnetic properties of the diluted magnetic semiconductor $\text{Sb}_{2-x}\text{Cr}_x\text{Te}_3$, *Phys. Rev. B* **71**, 115214 (2005).
- [16] Y. S. Hor, P. Roushan, H. Beidenkopf, J. Seo, D. Qu, J. G. Checkelsky, L. A. Wray, D. Hsieh, Y. Xia, S.-Y. Xu, D. Qian, M. Z. Hasan, N. P. Ong, A. Yazdani, and R. J. Cava, Development of ferromagnetism in the doped topological insulator $\text{Bi}_{2-x}\text{Mn}_x\text{Te}_3$, *Phys. Rev. B* **81**, 195203 (2010).
- [17] M. D. Watson, L. J. Collins-McIntyre, L. R. Shelford, A. I. Coldea, D. Prabhakaran, S. C. Speller, T. Mousavi, C. R. M. Grovenor, Z. Salman, S. R. Giblin, G. van der Laan, and T. Hesjedal, Study of the structural, electric and magnetic properties of Mn-doped Bi_2Te_3 single crystals, *New J. Phys.* **15**, 103016 (2013).
- [18] S. Zimmermann, F. Steckel, C. Hess, H. W. Ji, Y. S. Hor, R. J. Cava, B. Büchner, and V. Kataev, Spin dynamics and magnetic interactions of Mn dopants in the topological insulator Bi_2Te_3 , *Phys. Rev. B* **94**, 125205 (2016).
- [19] M. F. Islam *et al.*, Systematics of electronic and magnetic properties in the transition metal doped Sb_2Te_3 quantum anomalous Hall platform, *Phys. Rev. B* **97**, 155429 (2018).
- [20] D. Vaknin, D. M. Pajerowski, D. L. Schlagel, K. W. Dennis, and R. J. McQueeney, Two-dimensional ordering and collective magnetic excitations in the dilute ferromagnetic topological insulator $(\text{Bi}_{0.95}\text{Mn}_{0.05})_2\text{Te}_3$, *Phys. Rev. B* **99**, 220404(R) (2019).
- [21] J. Teng, N. Liu, and Y. Li, Mn-doped topological insulators: A review, *J. Semicond.* **40**, 081507 (2019).
- [22] J.-Q. Yan, S. Okamoto, M. A. McGuire, A. F. May, R. J. McQueeney, and B. C. Sales, Evolution of structural, magnetic, and transport properties in $\text{MnBi}_{2-x}\text{Sb}_x\text{Te}_4$, *Phys. Rev. B* **100**, 104409 (2019).
- [23] M. M. Otrokov *et al.*, Prediction and observation of an anti-ferromagnetic topological insulator, *Nature (London)* **576**, 416 (2019).
- [24] J. Li, Y. Li, S. Du, Z. Wang, B.-L. Gu, S.-C. Zhang, K. He, W. Duan, and Y. Xu, Intrinsic magnetic topological insulators in van der Waals layered MnBi_2Te_4 -family materials, *Sci. Adv.* **5**, eaaw5685 (2019).

- [25] D. Zhang, M. Shi, T. Zhu, D. Xing, H. Zhang, and J. Wang, Topological axion states in the magnetic insulator MnBi_2Te_4 with the quantized magnetoelectric effect, *Phys. Rev. Lett.* **122**, 206401 (2019).
- [26] C. Liu, Y. Wang, H. Li, Y. Wu, Y. Li, J. Li, K. He, Y. Xu, J. Zhang, and Y. Wang, Robust axion insulator and Chern insulator phases in a two-dimensional antiferromagnetic topological insulator, *Nat. Mater.* **19**, 522 (2020).
- [27] Y. J. Chen, L. X. Xu, J. H. Li, Y. W. Li, H. Y. Wang, C. F. Zhang, H. Li, Y. Wu, A. J. Liang, C. Chen, S. W. Jung, C. Cacho, Y. H. Mao, S. Liu, M. X. Wang, Y. F. Guo, Y. Xu, Z. K. Liu, L. X. Yang, and Y. L. Chen, Topological electronic structure and its temperature evolution in antiferromagnetic topological insulator MnBi_2Te_4 , *Phys. Rev. X* **9**, 041040 (2019).
- [28] J.-Q. Yan, Q. Zhang, T. Heitmann, Z. Huang, K. Y. Chen, J.-G. Cheng, W. Wu, D. Vaknin, B. C. Sales, and R. J. McQueeney, Crystal growth and magnetic structure of MnBi_2Te_4 , *Phys. Rev. Mater.* **3**, 064202 (2019).
- [29] Y. Gong *et al.*, Experimental realization of an intrinsic magnetic topological insulator, *Chinese Phys. Lett.* **36**, 076801 (2019).
- [30] Y. Deng, Y. Yu, M. Z. Shi, Z. Guo, Z. Xu, J. Wang, X. H. Chen, and Y. Zhang, Quantum anomalous Hall effect in intrinsic magnetic topological insulator MnBi_2Te_4 , *Science* **367**, 895 (2020).
- [31] Y.-J. Hao *et al.*, Gapless surface dirac cone in antiferromagnetic topological insulator MnBi_2Te_4 , *Phys. Rev. X* **9**, 041038 (2019).
- [32] S. H. Lee, Y. Zhu, Y. Wang, L. Miao, T. Pillsbury, H. Yi, S. Kempinger, J. Hu, C. A. Heikes, P. Quarterman, W. Ratcliff, J. A. Borchers, H. Zhang, X. Ke, D. Graf, N. Alem, C.-Z. Chang, N. Samarth, and Z. Mao, Spin scattering and non-collinear spin structure-induced intrinsic anomalous Hall effect in antiferromagnetic topological insulator MnBi_2Te_4 , *Phys. Rev. Res.* **1**, 012011(R) (2019).
- [33] W.-Z. Xu, C.-G. Chu, Z.-C. Pan, J.-J. Chen, A.-Q. Wang, Z.-B. Tan, P.-F. Zhu, X.-G. Ye, D.-P. Yu, and Z.-M. Liao, Proximity-induced superconducting gap in the intrinsic magnetic topological insulator MnBi_2Te_4 , *Phys. Rev. B* **105**, 184515 (2022).
- [34] H. Zhang, C. Q. Xu, S. H. Lee, Z. Q. Mao, and X. Ke, Thermal and thermoelectric properties of an antiferromagnetic topological insulator MnBi_2Te_4 , *Phys. Rev. B* **105**, 184411 (2022).
- [35] X. Kou, M. Lang, Y. Fan, Y. Jiang, T. Nie, J. Zhang, W. Jiang, Y. Wang, Y. Yao, L. He, and K. L. Wang, Interplay between different magnetisms in Cr-doped topological insulators, *ACS Nano* **7**, 9205 (2013).
- [36] Y. Tokura, K. Yasuda, and A. Tsukazaki, Magnetic topological insulators, *Nat. Rev. Phys.* **1**, 126 (2019).
- [37] F. Islam, Y. Lee, D. M. Pajerowski, J. Oh, W. Tian, L. Zhou, J. Yan, L. Ke, R. J. McQueeney, and D. Vaknin, Role of magnetic defects in tuning ground states of magnetic topological insulators, *Adv. Mater.* **35**, 2209951 (2023).
- [38] D. Vaknin, S. Pakhira, D. Schlagef, F. Islam, J. Zhang, D. M. Pajerowski, C. Z. Wang, D. C. Johnston, and R. J. McQueeney, Localized singlets and ferromagnetic fluctuations in the dilute magnetic topological insulator $\text{Sn}_{0.95}\text{Mn}_{0.05}\text{Te}$, *Phys. Rev. B* **101**, 140406(R) (2020).
- [39] J. B. Goodenough, *Magnetism and the Chemical Bond* (Interscience, New York, 1963).
- [40] M. Z. Hasan and C. L. Kane, *Colloquium: Topological insulators*, *Rev. Mod. Phys.* **82**, 3045 (2010).
- [41] X.-L. Qi and S.-C. Zhang, Topological insulators and superconductors, *Rev. Mod. Phys.* **83**, 1057 (2011).
- [42] T. H. Hsieh, H. Lin, J. Liu, W. Duan, A. Bansil, and L. Fu, Topological crystalline insulators in the SnTe material class, *Nat. Commun.* **3**, 982 (2012).
- [43] Y. Tanaka, Z. Ren, T. Sato, K. Nakayama, S. Souma, T. Takahashi, K. Segawa, and Y. Ando, Experimental realization of a topological crystalline insulator in SnTe, *Nat. Phys.* **8**, 800 (2012).
- [44] S.-Y. Xu *et al.*, Observation of a topological crystalline insulator phase and topological phase transition in $\text{Pb}_{1-x}\text{Sn}_x\text{Te}$, *Nat. Commun.* **3**, 1192 (2012).
- [45] P. Dziawa, B. J. Kowalski, K. Dybko, R. Buczko, A. Szczerbakow, M. Szot, E. Łusakowska, T. Balasubramanian, B. M. Wojek, M. H. Berntsen, O. Tjernberg, and T. Story, Topological crystalline insulator states in $\text{Pb}_{1-x}\text{Sn}_x\text{Se}$, *Nat. Mater.* **11**, 1023 (2012).
- [46] P. Bauer Pereira, I. Sergueev, S. Gorsse, J. Dadda, E. Müller, and R. P. Hermann, Lattice dynamics and structure of GeTe, SnTe and PbTe, *Phys. Status Solidi B* **250**, 1300 (2013).
- [47] M. Inoue, K. Ishii, and H. Yagi, Ferromagnetic ordering in Mn-doped SnTe crystals, *J. Phys. Soc. Jpn.* **43**, 903 (1977).
- [48] C. W. H. M. Vennix, E. Frikkee, P. J. T. Eggenkamp, H. J. M. Swagten, K. Kopinga, and W. J. M. de Jonge, Neutron-diffraction study of the carrier-concentration-induced ferromagnet-to-spin-glass transition in the diluted magnetic semiconductor $\text{Sn}_{1-x}\text{Mn}_x\text{Te}$, *Phys. Rev. B* **48**, 3770 (1993).
- [49] P. J. T. Eggenkamp, C. W. H. M. Vennix, T. Story, H. J. M. Swagten, C. H. W. Swüste, and W. J. M. De Jonge, Magnetic study of the diluted magnetic semiconductor $\text{Sn}_{1-x}\text{Mn}_x\text{Te}$, *J. Appl. Phys.* **75**, 5728 (1994).
- [50] C.-Z. Chang, C.-X. Liu, and A. H. MacDonald, *Colloquium: Quantum anomalous Hall effect*, *Rev. Mod. Phys.* **95**, 011002 (2023).
- [51] M. Inoue, H. Oshima, M. Morisaki, H. Yagi, H. Kun Fun, and T. Tatsukawa, Various types of magnetism in SnTe crystals doped with 3D transition metals, *J. Phys. Soc. Jpn.* **50**, 1222 (1981).
- [52] F. Wang, H. Zhang, J. Jiang, Y.-F. Zhao, J. Yu, W. Liu, D. Li, M. H. W. Chan, J. Sun, Z. Zhang, and C.-Z. Chang, Chromium-induced ferromagnetism with perpendicular anisotropy in topological crystalline insulator SnTe (111) thin films, *Phys. Rev. B* **97**, 115414 (2018).
- [53] Y. Muhammad, H. Yin, G. Zhang, H. Wu, L. Zhang, L. Yang, L. Li, I. Tahir, R. Hasan, S. Atiq, W. Zhang, and H. Chang, Highly tunable beyond-room-temperature intrinsic ferromagnetism in Cr-doped topological crystalline insulator SnTe crystals, *Inorg. Chem.* **61**, 19702 (2022).
- [54] See Supplemental Material at <http://link.aps.org/supplemental/10.1103/PhysRevB.110.014408> for details of sample synthesis and characterization, extended elastic neutron scattering data, extended Q dependencies, inelastic neutron scattering intensity, details of first-principles calculations; and band-filling evaluation of magnetic interactions.
- [55] B. Hennion, W. Szuszkiewicz, E. Dynowska, E. Janik, and T. Wojtowicz, Spin-wave measurements on MBE-grown zinc-blende structure MnTe by inelastic neutron scattering, *Phys. Rev. B* **66**, 224426 (2002).
- [56] W. Szuszkiewicz, E. Dynowska, B. Witkowska, and B. Hennion, Spin-wave measurements on hexagonal MnTe of

- NiAs-type structure by inelastic neutron scattering, *Phys. Rev. B* **73**, 104403 (2006).
- [57] T. Gawron and M. Cieplak, Site percolation thresholds of FCC lattice, *Acta Phys. Pol. A* **80**, 461 (1991).
- [58] Y. Lai, L. Ke, J. Yan, R. D. McDonald, and R. J. McQueeney, Defect-driven ferrimagnetism and hidden magnetization in MnBi_2Te_4 , *Phys. Rev. B* **103**, 184429 (2021).
- [59] G. Kresse and D. Joubert, From ultrasoft pseudopotentials to the projector augmented-wave method, *Phys. Rev. B* **59**, 1758 (1999).
- [60] G. Kresse and J. Furthmüller, Efficiency of *ab-initio* total energy calculations for metals and semiconductors using a plane-wave basis set, *Comp. Mater. Sci.* **6**, 15 (1996).
- [61] J. P. Perdew, K. Burke, and M. Ernzerhof, Generalized gradient approximation made simple, *Phys. Rev. Lett.* **77**, 3865 (1996).
- [62] P. Blaha, K. Schwarz, and G. K. H. Madsen, *WIEN2k: An Augmented Plane Wave Plus Local Orbitals Program for Calculating Crystal Properties* (Vienna University of Technology, Vienna, 2018).
- [63] L. Ke and M. van Schilfgaarde, Band-filling effect on magnetic anisotropy using a Green's function method, *Phys. Rev. B* **92**, 014423 (2015).
- [64] D. Khomskii and G. Sawatzky, Interplay between spin, charge and orbital degrees of freedom in magnetic oxides, *Solid State Commun.* **102**, 87 (1997).
- [65] J. Deisenhofer, M. Paraskevopoulos, H.-A. Krug von Nidda, and A. Loidl, Interplay of superexchange and orbital degeneracy in Cr-doped LaMnO_3 , *Phys. Rev. B* **66**, 054414 (2002).
- [66] J. Xin, S. Li, J. Yang, A. Basit, Q. Long, S. Li, Q. Jiang, T. Xu, and B. Xiao, Tactfully decoupling interdependent electrical parameters via interstitial defects for SnTe thermoelectrics, *Nano Energy* **67**, 104292 (2020).
- [67] L. Ke and M. I. Katsnelson, Electron correlation effects on exchange interactions and spin excitations in 2D van der Waals materials, *npj Comput. Mater.* **7**, 4 (2021).
- [68] R. McQueeney, Coexistence of ferromagnetism and antiferromagnetic dimers in topological insulators, <https://doi.org/10.7910/DVN/1ZYPZT>, Harvard Dataverse, V1 (2024).